Acta Crystallographica Section D
Biological Crystallography
ISSN 0907-4449

Structural studies on the folded domain of the human prion protein bound to the Fab fragment of the antibody POM1

Pravas Kumar Baral,[a] Barbara Wieland,[a,b] Mridula Swayampakula,[a,b] Magdalini Polymenidou,[c,d] Muhammad Hafiz Rahman,[b] Nat N. V. Kav,[b] Adriano Aguzzi[d] and Michael N. G. James[a]*

[a]Department of Biochemistry, School of Translational Medicine, Faculty of Medicine and Dentistry, University of Alberta, Edmonton AB T6G 2H7, Canada, [b]Department of Agricultural, Food and Nutritional Science, University of Alberta, Edmonton AB T6G 2P5, Canada, [c]Department of Cellular and Molecular Medicine, University of California at San Diego, La Jolla, CA 92093-0670, USA, and [d]Department of Pathology, Institute of Neuropathology, University Hospital Zurich, Zurich, Switzerland

Correspondence e-mail: michael.james@ualberta.ca

Received 28 May 2012
Accepted 29 August 2012

PDB Reference: POM1 Fab–huPrP^{c} complex, 4dgi

Prion diseases are neurodegenerative diseases characterized by the conversion of the cellular prion protein PrP^{c} into a pathogenic isoform PrP^{sc}. Passive immunization with antiprion monoclonal antibodies can arrest the progression of prion diseases. Here, the crystal structure of the Fab fragment of an antiprion monoclonal antibody, POM1, in complex with human prion protein (huPrP^{c}) has been determined to 2.4 Å resolution. The prion epitope of POM1 is in close proximity to the epitope recognized by the purportedly therapeutic antibody fragment ICSM18 Fab in complex with huPrP^{c}. POM1 Fab forms a 1:1 complex with huPrP^{c} and the measured K_{d} of 4.5×10^{-7} M reveals moderately strong binding between them. Structural comparisons have been made among three prion–antibody complexes: POM1 Fab–huPrP^{c}, ICSM18 Fab–huPrP^{c} and VRQ14 Fab–ovPrP^{c}. The prion epitopes recognized by ICSM18 Fab and VRQ14 Fab are adjacent to a prion glycosylation site, indicating possible steric hindrance and/or an altered binding mode to the glycosylated prion protein *in vivo*. However, both of the glycosylation sites on huPrP^{c} are positioned away from the POM1 Fab binding epitope; thus, the binding mode observed in this crystal structure and the binding affinity measured for this antibody are most likely to be the same as those for the native prion protein *in vivo*.

1. Introduction

Prion diseases affect a variety of mammalian species and are collectively known as transmissible spongiform encephalopathies (TSEs); they include bovine spongiform encephalopathy (BSE) in cattle, chronic wasting disease (CWD) in cervids, scrapie in sheep and goats and Creutzfeldt–Jakob disease (CJD) in humans (Aguzzi & Polymenidou, 2004). These are progressively degenerative disorders of the central nervous system that result in motor dysfunction, dementia and ultimately death (Collinge, 2001). Different fatal forms of human prion diseases are also known; these are kuru, variant Creutzfeldt–Jakob disease (vCJD), Gerstmann–Straussler–Scheinker syndrome (GSS) and fatal familial insomnia (FFI) (Collinge, 2001). The hallmark of prion diseases is the accumulation of amyloid fibrils in the brain tissue, resulting in excessive neuronal degeneration and spongiosis (Will, 1999). The conversion of normal cellular prion protein (PrP^{c}), which is ubiquitously expressed in the human body and is especially abundant in brain tissue, into a pathogenic conformation (PrP^{sc}) is the crucial step in the onset of this disease. This pathogenic prion conformation, PrP^{sc}, possesses abnormal physicochemical properties such as resistance to proteolytic degradation, insolubility and a propensity to polymerize into amyloid-like fibrils. According to the 'protein-only'

hypothesis, transmission of TSEs is completely a PrP^{sc}-dependent phenomenon; PrP^{sc} acts as a template for its self-propagation as well as for its replication through recruiting normal cellular prion molecules and the cycle continues, leading to the formation of amyloid fibrils (Sigurdson *et al.*, 2009; Castilla *et al.*, 2005). During this PrP^{sc} conversion process the helical nature of the cellular prion protein is almost completely lost, giving rise to β-strands and turns, which then aggregate amongst themselves, forming long extended fibril-like structures (Smirnovas *et al.*, 2011).

Until now there has been no treatment available either to cure or to halt the progression of prion diseases; however, any interruption in the pathogenic conversion process of PrP^{c} to PrP^{sc} at the neuronal level could potentially prevent the progression of these diseases (White *et al.*, 2003). One of the therapeutic approaches considered for the treatment of prion diseases has been the use of antiprion monoclonal antibodies as a passive immunization agent that could possibly reduce PrP^{sc} accumulation by disrupting the vicious pathological cycle of PrP^{c}-to-PrP^{sc} conversion (White *et al.*, 2003; Antonyuk *et al.*, 2009). The proposed mechanism by which these antibodies may reduce levels of PrP^{sc} is that antiprion monoclonal antibodies bind to the PrP^{c} molecule and stabilize it in its native conformation through tight binding, thus preventing any untoward conformational changes. A different conformation of the prion molecule, known as βPrP, has been implicated in initiation of PrP^{sc} formation and prion propagation (Hosszu *et al.*, 2009). Several *in vitro* and *in vivo* studies of antiprion monoclonal antibodies have been reported to reduce the amount of scrapie prion (White *et al.*, 2003; Féraudet *et al.*, 2005). Furthermore, an *in vivo* study in a murine model also suggested a delay in the development of prion disease after inoculation with two antiprion antibodies: ICSM18 and ICSM35 (White *et al.*, 2003). A separate study on cell-surface PrP^{c} revealed that this protein acts as the cellular receptor for amyloid Aβ oligomer (Kessels *et al.*, 2010), the key element in the pathophysiological process of Alzheimer's disease. The pathogenic association of PrP^{c} and the Aβ oligomer is the leading cause of synaptic dysfunction, as observed in Alzheimer's disease (Calella *et al.*, 2010). Hence, disruption of this toxic interaction, with the help of PrP^{c}-specific monoclonal antibodies, could be an appropriate therapeutic approach that can be targeted against both prion and Alzheimer's diseases (Kessels *et al.*, 2010; Freir *et al.*, 2011). However, the use of antiprion antibodies as a passive immunization agent cannot be considered absolutely without risk, as there are a few inconsistent observations regarding the safety of these agents. Two antiprion monoclonal antibodies, IgG D13 and IgG P, can cause extensive neuronal loss upon *in vivo* administration in the mouse brain hippocampus (Solforosi *et al.*, 2004). Although the exact molecular mechanism of antibody-mediated toxicity is not clear, cross-linking of the antibody has been reported to be the factor responsible for this toxicity. In another comparative analysis recently performed by Klohn and coworkers, *in vivo* administration of several antiprion antibodies, IgG D13, IgG P, IgG ICSM18 and IgG ICSM35, into the left hippocampus of mouse brain indicated that these monoclonal antibodies are nontoxic (Klöhn *et al.*, 2012). Therefore, the current challenge for the development of prion therapeutics is to find tight-binding monoclonal antibodies that are also safe for *in vivo* administration. Structural studies on antiprion antibodies bound to PrP^{c} molecules will provide essential insights in this regard by deciphering the structural features that are responsible for tighter association. However, until now, few attempts have been made to crystallize antiprion monoclonal antibodies bound to their cognate PrP^{c} molecules. The crystal structures of two Fab fragments of monoclonal antibodies bound to the cognate C-terminal parts of prion proteins are available in the PDB: the Fab fragment of a potentially therapeutic antibody ICSM18 bound to human PrP^{c} (residues 119–231; PDB entry 2w9e; Antonyuk *et al.*, 2009) and the Fab fragment of antibody VRQ14 bound to ovine PrP^{c} (residues 114–234; PDB entry 1tpx; Eghiaian *et al.*, 2004).

19 antiprion monoclonal antibodies, POM1–POM19, were produced against recombinant mouse PrP^{c} ($moPrP^{c}$) using a prion-knockout mouse strain; among these antibodies, several recognize the conformationally structured C-terminal domain of PrP^{c} (Polymenidou *et al.*, 2008). Here, we report structural studies on an antibody fragment, POM1 Fab, in complex with the C-terminal folded domain of human PrP^{c} ($huPrP^{c}$; residues 120–230). In addition to these structural data, thermodynamic binding studies on POM1 Fab and $huPrP^{c}$ suggest a moderately strong association between them. The antibody fragment POM1 Fab recognizes a portion of the $huPrP^{c}$ epitope helix α1. Interestingly, the purportedly therapeutic antibody fragment ICSM18 Fab also recognizes the $huPrP^{c}$ epitope helix α1, although the binding modes of these two antibodies towards $huPrP^{c}$ are vastly different. Based on the available structural data for different prion–antibody complexes, the nature of the intermolecular interactions between PrP^{c}s and their cognate antibody partners are compared. Structural analyses of prion–antibody complexes will play a key role in the design of therapeutic products against prion diseases.

2. Materials and methods

2.1. Production and purification of recombinant PrP^{c}

The cDNA encoding the C-terminal part of human PrP^{c} ($huPrP^{c}$; residues 120–230), mouse PrP^{c} ($moPrP^{c}$; residues 90–231), bovine PrP^{c} ($boPrP^{c}$; residues 103–242) and sheep PrP^{c} ($ovPrP^{c}$; residues 94–233) were cloned in a pET15b plasmid and transformed in *Escherichia coli* BL21 (DE3) (Stratagene) cells. These PrP^{c} genes contain a His_6 affinity tag fused at the C-terminus and preceded by a thrombin cleavage site that allows removal of the affinity tag after protein purification. The cells were grown in rich medium containing 0.1 mg ml^{-1} ampicillin at 310 K and the prion proteins were expressed mainly in the form of inclusion bodies. The cells were pelleted by centrifugation at 8000 rev min^{-1} for 20 min, taken up in 50 m*M* Tris, 200 m*M* NaCl pH 8.0 and the homogeneous solution was then sonicated (4 × 30 s with a 60 s interval at

50% amplitude). The inclusion bodies were spun down at 27 000*g* for 30 min and the pellet was extensively washed with 2% sodium deoxycholate in 50 m*M* Tris, 200 m*M* NaCl pH 8.0 followed by four buffer washes without detergent. Subsequently, the inclusion bodies were incubated in a denaturing buffer consisting of 6 *M* guanidinium hydrochloride, 10 m*M* Tris–HCl, 100 m*M* NaH_2PO_4, 5 m*M* imidazole pH 8.0 for 1 h at room temperature with constant stirring. The extracted denatured prion proteins were then loaded onto an Ni–NTA agarose column (Qiagen) at a flow rate of 1 ml min^{-1} after the addition of 10 m*M* reduced glutathione. The prion proteins were refolded on the column by gradient application of buffer *A* (denaturing buffer) and buffer *B* (10 m*M* Tris–HCl, 100 m*M* NaH_2PO_4, 5 m*M* imidazole pH 8.0) as described by Yin *et al.* (2003). Finally, the prion proteins were eluted with 300 m*M* imidazole in buffer *B* at pH 5.8, exchanged with distilled water and concentrated using Amicon Ultra centrifugal filters (3 kDa molecular-weight cutoff, Millipore). The His_6 affinity tag of the huPrP^c was removed by digestion with thrombin at a huPrP^c:thrombin ratio of 1:0.02(*w*:*w*) in 50 m*M* Tris pH 8.0, 150 m*M* NaCl, 2 m*M* EDTA at 303 K in a water bath overnight. The purity of these prion proteins was confirmed by SDS–PAGE and their concentration was measured by the Bradford method (Bradford, 1976) using bovine serum albumin as a standard.

2.2. POM1 Fab fragment production

The IgG1 POM1 hybridoma was prepared according to Polymenidou *et al.* (2008). After hybridoma cell culture, the antibody-enriched and cell-free medium was loaded onto a Protein G Sepharose column and the POM1 antibody was eluted with 0.1 *M* glycine pH 2.8. For Fab production, the POM1 IgG1 (1 mg ml^{-1}) was digested with papain at a POM1:papain ratio of 1:0.02(*w*:*w*) in 50 m*M* Tris pH 8.0, 150 m*M* NaCl, 20 m*M* EDTA, 20 m*M* cysteine. The papain enzyme was inactivated by the addition of 30 m*M* iodoacetamide after 5 h incubation at 310 K in a water bath. The POM1 digest was then concentrated and buffer-exchanged with Protein A IgG-binding buffer (Thermo Scientific) and loaded onto a Protein A Sepharose column (Pierce). The Fc fragment and undigested POM1 IgG1 remained bound to the Protein A column, whereas the POM1 Fab fragments were collected in the flowthrough. The Fab fractions were exchanged with 50 m*M* Tris, 150 m*M* NaCl pH 8.0, concentrated and finally assessed for homogeneity by Coomassie Brilliant Blue staining after separation by SDS–PAGE.

2.3. Purification and crystallization of POM1 Fab–huPrP^c

POM1 Fab and huPrP^c were mixed in an equimolar ratio in order to form the protein complex; the resulting complex was subsequently purified by Superdex G-75 (Amersham Biosciences) size-exclusion chromatography in a buffer solution consisting of 50 m*M* Tris pH 7.0, 100 m*M* NaCl, 1 m*M* NaN_3. For crystallization studies, the purified protein complex was concentrated to a final concentration of 10 mg ml^{-1}. Screening of crystallization conditions for the POM1 Fab–huPrP^c complex was carried out using several commercial screening solutions from Hampton Research in 96-well Intelli-Plates (Hampton Research) with the aid of a crystallization robot (Hydra 96 Plus One, Robbins Scientific). Crystallization trays were set up by the sitting-drop vapour-diffusion method, in which 0.4 µl protein sample was mixed with an equal volume of screening solution. An initial crystallization hit was found in a saturating solution of 25% PEG 3350, 0.1 *M* MES pH 6.5, 0.1 *M* sodium acetate. After a few optimization steps similar to those used to obtain diffraction-quality crystals of the POM1 Fab–moPrP^c complex, POM1 Fab–huPrP^c protein-complex crystals were obtained within 7 d with approximate dimensions of 0.6 × 0.2 × 0.3 mm (Baral *et al.*, 2011).

Table 1
Summary of crystallographic data-collection and refinement statistics for the POM1 Fab–huPrP^c complex.

Values in parentheses are for the highest resolution shell.

Data-collection statistics	
Space group	*C*2
Resolution (Å)	76.5–2.4 (2.53–2.40)
Completeness (%)	99.3 (99.3)
R_{merge}†	0.19 (0.78)
$\langle I/\sigma(I)\rangle$	6.8 (2.3)
Multiplicity	3.8 (3.8)
Total No. of reflections	100576
Unique reflections	26309
Unit-cell parameters	
a (Å)	83.53
b (Å)	105.92
c (Å)	76.23
β (°)	95.08
Solvent content (%)	58
Refinement statistics	
Final R_{cryst}‡ (%)	25.6
R_{free}‡ (%)	28.9
No. of atoms	
Total	4276
Protein	4105
Ions	1
Water molecules	170
B factors (Å^2)	
Average	63.9
Protein	63.9
Ions	23.4
Water molecules	43.0
R.m.s.d.	
Bond lengths (Å)	0.017
Bond angles (°)	2.006

† $R_{merge} = \sum_{hkl}\sum_i |I_i(hkl) - \langle I(hkl)\rangle| / \sum_{hkl}\sum_i I_i(hkl)$, where $\langle I(hkl)\rangle$ is the mean intensity for multiply recorded reflections. ‡ R_{work} and $R_{free} = \sum_{hkl} \big||F_{obs}| - |F_{calc}|\big| / \sum_{hkl} |F_{obs}|$ for reflections in the working and test (5% of the data) sets.

2.4. Data collection and structure determination

The POM1 Fab–huPrP^c complex crystals were picked up directly from the sitting drop for data collection; 20% glycerol was used as a cryoprotecting solution. Intensity data were collected at the Canadian Light Source, Saskatoon, Saskatchewan. Data were processed using the *MOSFLM* program (Leslie, 2006). The data-collection details and the refinement statistics are presented in Table 1. The protein-complex structure was solved by the molecular-replacement method using the program *MOLREP* (Vagin & Teplyakov, 2010) in the *CCP*4 package (Winn *et al.*, 2011). An Fab

structure from the PDB (PDB entry 2w9e; Antonyuk *et al.*, 2009) was used as the search model for the Fab molecule in the POM1 Fab–huPrP^{c} complex. The prion protein was then searched for in the POM1 Fab–huPrP^{c} complex using the coordinates of human prion protein (PDB entry 3hak; Lee *et al.*, 2010) as the search model. Models were refined using the refinement program of the *PHENIX* package (Afonine *et al.*, 2012). The progress of the refinement process was monitored by reduction of both the R and $R_{\rm free}$ factors. Solvent molecules were added to the model in an automated manner in *PHENIX* and water molecules were accepted only when well defined positive peaks were present in both $2|F_{\rm o}| - |F_{\rm c}|$ and $|F_{\rm o}| - |F_{\rm c}|$ electron-density maps and there was a satisfactory hydrogen-bonding network with either protein atoms or other water molecules. Model building was performed with the program *Coot* (Emsley & Cowtan, 2004). The coordinates and the structure factors for the POM1 Fab–huPrP^{c} complex have been deposited in the PDB as entry 4dgi.

2.5. Isothermal titration calorimetry

A VP-ITC microcalorimeter (Microcal, Northampton, Massachusetts, USA) was used to analyze the binding of POM1 Fab and huPrP^{c}. The proteins were dialyzed against 50 m*M* NaH_2PO_4 pH 6.0, 200 m*M* NaCl and degassed prior to analysis. POM1 Fab was injected into the sample cell and huPrP^{c} (50 µ*M* solutions) was placed into the syringe, or *vice versa* with the exception that a slightly higher concentration of POM1 Fab was used (60 µ*M*). The dialysis buffer was placed in the reference cell. Either POM1 Fab or huPrP^{c} was titrated against the dialysis buffer to obtain the heat of dilution. The following parameters were used in the titration: 303 K, 10 µl injections and 4 min between injections with stirring at 305 rev min^{-1}. The titration data were fitted using *Origin* v.5.0 (MicroCal) to extract the thermodynamic parameters.

2.6. ELISA

The antibody fragment POM1 Fab, generated by papain digestion of POM1 IgG1 from the mouse hybridoma, was immobilized on the solid surface of the wells of a 96-well plate at a concentration of 0.01 mg ml^{-1} and was incubated overnight at 277 K. Unoccupied hydrophobic sites on the surfaces of the plastic wells were blocked by the application of 3%(*w*/*v*) BSA in PBS buffer pH 7.2 at room temperature for 2 h. Excess reactants were washed away with PBS buffer containing 0.05% Tween-20, followed by several washes with PBS buffer only. Recombinant polyhistidine-tagged fusion prion protein analytes from mouse (moPrP^{c} 90–231), bovine (boPrP^{c} 103–242) and sheep (ovPrP^{c} 90–230) were added to the wells at increasing dilutions in 3% BSA and PBS buffer and were subsequently incubated for 2 h at room temperature with gentle shaking. After washing as described previously, His-Probe-HRP (Thermo Scientific) at a dilution of 1:5000 was added and the plate was kept at room temperature for 1 h. For colour detection, SureBlue Reserve TMB Microwell Peroxidase Substrate (1-Component) was added after washing and the reaction was stopped after 10 min by the addition of 1 *M*

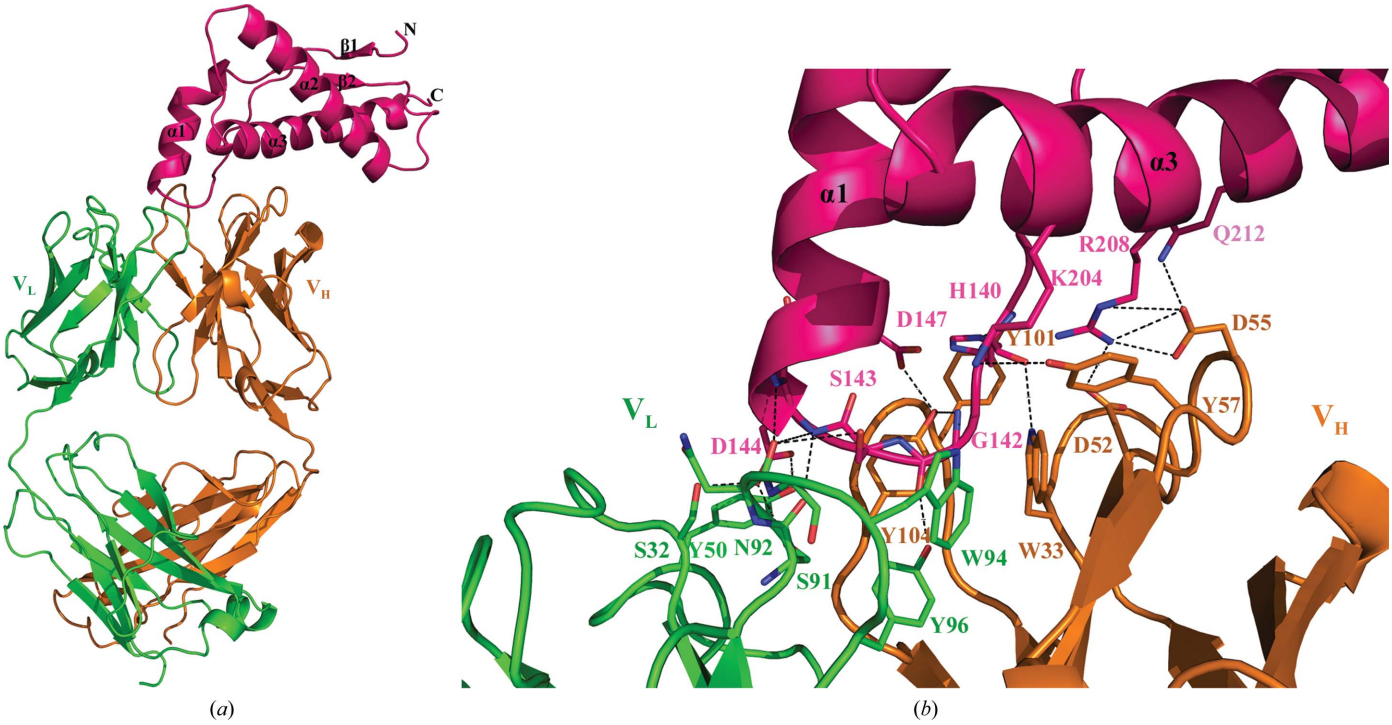

Figure 1
The crystal structure of the protein complex between the C-terminal domain of the recombinant human prion protein (120–230) and POM1 Fab. (*a*) The human prion protein is shown in magenta; the heavy chain and the light chain of POM1 Fab are represented in orange and green, respectively. (*b*) A close-up of the intermolecular contacts between POM1 Fab and the human prion protein. Hydrogen-bonding interactions are shown as dashed lines (distances are given in Table 3).

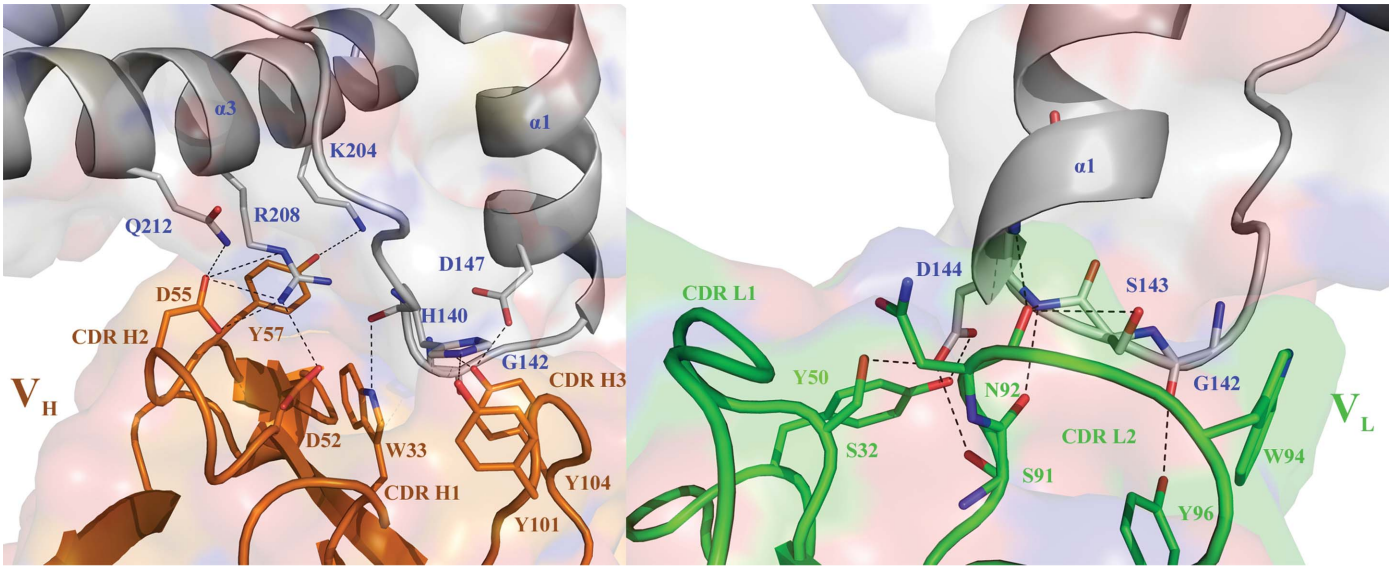

(*a*) (*b*)

Figure 2
Intermolecular contacts between the surface of human prion protein and POM1 Fab. (*a*) Human prion protein (grey) with POM1 Fab variable heavy chain (magenta). (*b*) Human prion protein (grey) with POM1 Fab variable light chain (green).

HCl. Subsequently, the absorbance was measured at a wavelength of 450 nm using a SpectraMax 190 microplate reader (Molecular Devices Corporation).

3. Results

The intermolecular contacts between huPrP^{c} and the POM1 Fab have been investigated by determining the crystal structure of the folded C-terminal domain of huPrP^{c} (120–230) in complex with the Fab fragment of POM1 at a resolution of 2.4 Å (Fig. 1*a*, Table 1 and Supplementary Table S1[1]). The overall fold of the C-terminal domain of huPrP^{c} consists of two short antiparallel β-strands (residues 129–131 and 161–163) and three α-helices (residues 146–158, 174–196 and 203–230). Electron density for the six N-terminal residues (residues 120–125) and the seven C-terminal residues (residues 223–230) of huPrP^{c} was not visible in the electron-density map. The crystallographic data have a high average *B* factor because certain regions of the protein complex, especially the constant domains of both the POM1 Fab light chain and the POM1 Fab heavy chain, are less well ordered. However, the binding interface between huPrP^{c} and the POM1 Fab is relatively well ordered. The structural fold observed for huPrP^{c} bound to the POM1 Fab is similar to the available X-ray structures in the PDB and to the various NMR structures of huPrP^{c} proteins. Structural superposition of the huPrP^{c} protein bound to POM1 Fab with huPrP^{c} solved by X-ray crystallography (PDB entry 3hak; Lee *et al.*, 2010) and by NMR spectroscopy (PDB entry 1qm1; Zahn *et al.*, 2000) revealed overall root-mean-square deviations (r.m.s.d.s) of 1.0 and 1.8 Å, respectively, for the main-chain C$^{\alpha}$ atoms in the residue range 125–223 (Table 2 and Supplementary Fig. S1[1]). However, striking differences have been observed between this monomeric form of the huPrP^{c} protein structure bound to an antibody Fab fragment and the crystal structure of a domain-swapped dimeric huPrP^{c} protein (PDB entry 1i4m; Knaus *et al.*, 2001). In the dimeric huPrP^{c} conformation, helix α3 from one monomer is swapped with helix α3 from the other monomer of the dimer by forming two intermolecular disulfide bridges, unlike the single intramolecular disulfide bridge present between helix α3 and helix α2 of the huPrP^{c} monomer (Knaus *et al.*, 2001).

3.1. Structure of the POM1 Fab–huPrP^{c} complex

The globular folded domain of huPrP^{c} interacts with the POM1 Fab mainly through the C-terminal part of the loop joining strand β1 and helix α1 (residues 140–147). The secondary binding epitope for the POM1 Fab involves three noncontiguous residues, Lys204, Arg208 and Gln212, on helix α3 of huPrP^{c} (Fig. 1*b*). This discontinuous prion epitope observed for the POM1 Fab is partially in agreement with the previous epitope-mapping experiment, which revealed helix α1 to be the primary epitope (Polymenidou *et al.*, 2008). Formation of the POM1 Fab–huPrP^{c} complex buries a surface area of 580 Å^{2}, which is ∼9% of the total accessible surface area of the ordered folded domain of huPrP^{c}. The major portion of this interaction interface is contributed by the heavy chain of the POM1 Fab. Several residues from the three complementarity-determining regions (CDRs) of the POM1 Fab heavy chain (CDR H1, residues 25–33; CDR H2, residues 52–56; CDR H3, residues 98–107) are in contact with the huPrP^{c} protein (Fig. 2*a*). Two neighbouring negatively charged residues from CDR H2, Asp52 and Asp55, form salt-bridge interactions with a positively charged residue, Arg208, of huPrP^{c}. These partially buried salt bridges, Arg208–Asp52 and Arg208–Asp55, are present in the interface of POM1 Fab and

[1] Supplementary material has been deposited in the IUCr electronic archive (Reference: RR5023). Services for accessing this material are described at the back of the journal.

Table 2
Root-mean-square deviation (r.m.s.d.) in Å for backbone superimposition of PrP^{c}s.

The main-chain atoms (residues 126–222) of the huPrP^c X-ray structure (PDB entry 3hak; Lee *et al.*, 2010), the huPrP^c NMR structure (PDB entry 1qm1; Zahn *et al.*, 2000), POM1 Fab–huPrP^c (this work), ICSM18 Fab–huPrP^c (PDB entry 2w9e; Antonyuk *et al.*, 2009) and VRQ14 Fab–ovPrP^c (residues 129–225; PDB entry 1tpx; Eghiaian *et al.*, 2004) were used for these superpositions.

	huPrP^c, X-ray	huPrP^c, NMR	POM1 Fab–huPrP^c	ICSM18 Fab–huPrP^c	VRQ14 Fab–ovPrP^c
huPrP^c, X-ray	0.0	1.82	1.00	1.07	1.14
huPrP^c, NMR		0.0	1.85	1.72	1.82
POM1 Fab–huPrP^c			0.0	0.93	0.89
ICSM18 Fab–huPrP^c				0.0	0.81
VRQ14 Fab–ovPrP^c					0.0

Table 3
Summary of interactions between huPrP^c and POM1 Fab in the crystal structure.

huPrP^c	POM1 Fab	Distance (Å)
POM1 Fab light chain		
Gly142 O	Tyr96 OH	2.3
Ser143 OH	Asn92 O	3.4
Asp144 OD2	Ser32 OH	2.4
Asp144 OD2	Ser91 OH	3.3
Asp144 N	Ser91 O	2.8
Asp 144 OD1	Tyr50 OH	2.6
Asp144 N	Asn92 O	3.4
Tyr145 N	Asn92 O	3.0
POM1 Fab heavy chain		
His140 O	Trp33 NE1	3.3
His140 NE2	Tyr101 OH	3.5
Gly142 N	Tyr104 OH	3.3
Asp147 OD2	Tyr104 OH	2.9
Lys204 NZ	Tyr57 OH	3.9
Arg208 NH1	Asp52 OD2	2.8
Arg208 NH1	Asp55 OD1	3.2
Arg208 NH1	Asp55 OD2	3.1
Arg208 NE	Asp55 OD2	2.8
Gln212 NE2	Asp55 OD2	3.0

huPrP^c; the latter salt bridge forms three hydrogen bonds owing to excellent geometry between the oppositely charged residues (Fig. 2*a* and Table 3). Although hydrophobicity is viewed as the major force in protein–protein interactions, electrostatic forces still make an important contribution towards the association rate and this defines the lifetime of a complex (Sinha & Smith-Gill, 2002). Additionally, the guanidium group of Arg208 also participates in a cation–π interaction (Crowley & Golovin, 2005) with the aromatic ring of Tyr57, which is also part of the CDR H2 region. The distance between the plane of the guanidinium group and the aromatic ring centre is ∼3.5 Å; this interaction between the CDR H2 paratope and the helix α3 epitope is strengthened by an additional hydrogen bond between the hydroxyl group of Tyr57 and the protonated N$^{\varepsilon}$ atom of Lys204. Two aromatic residues in the CDR H3 region, Tyr101 and Tyr104, make

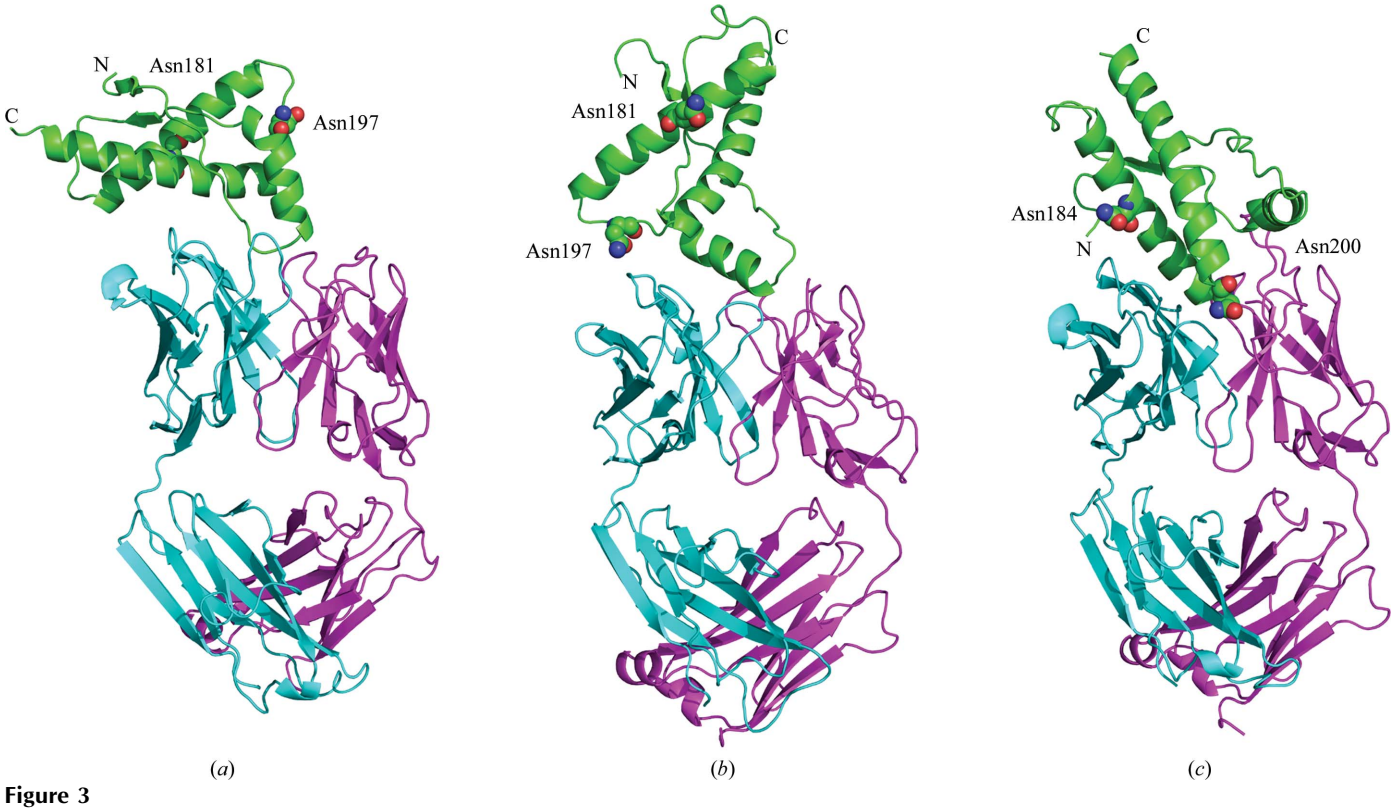

Figure 3
The structures of recombinant human and sheep prion proteins bound to antibody Fab fragments. The prion proteins are shown in green and the light chain and the heavy chain of the bound Fab fragments are represented in magenta and cyan, respectively. The *N*-glycosylation sites on the prion proteins are shown as spheres. (*a*) Human prion protein with POM1 Fab. (*b*) Human prion protein with ICSM18 Fab (Antonyuk *et al.*, 2009). (*c*) Sheep prion protein with VRQ14 Fab (Eghiaian *et al.*, 2004).

hydrogen bonds to residues His140 and Asp147 of the huPrP^{c} protein. The abundance of aromatic and hydrophobic side chains in antigen–antibody interaction interfaces and their functional role during protein-complex formation has been well established (Ramaraj *et al.*, 2012).

Compared with the heavy chain, the light chain makes a considerably smaller contribution towards the prion–antibody interaction. Only a few residues of the POM1 Fab light chain CDR L2 (residues 90–102) make contact with the N-terminal part of helix α1: Ser91, Asn92 and Tyr96 (Fig. 2*b*). The main-chain atoms of both interacting partners are involved in these contacts; the carbonyl groups of Ser91 and Asn92 of the POM1 Fab light chain CDR L2 region form hydrogen bonds to the main-chain amide N atoms of huPrP^{c} residues Asp144 and Tyr145, respectively. The positive end of the N-terminal part of helix α1 seems to be stabilized through the backbone carbonyl groups of the CDR L2. Additionally, the hydroxyl groups of Tyr96 and Ser91 of the CDR L2 are also in contact with the main-chain carbonyl group of Gly142 and the carboxylate group of Asp144 of huPrP^{c}. Two other residues, Ser32 of the POM1 Fab light chain CDR L1 (residue range 25–33) and Tyr50, make contact with Asp144 of the huPrP^{c} protein (Fig. 2*b* and Table 3). In addition to several hydrogen-bonding interactions between the interacting partners, two tryptophan residues, one from the light chain and one from the heavy chain, Trp94 and Trp33, provide a hydrophobic environment for protein-complex formation.

3.2. Structural comparisons among different antibody Fab–PrP^{c} complexes

Three different binding modes for the folded C-terminal parts of the prion proteins are observed in the POM1 Fab–huPrP^{c}, ICSM18 Fab–huPrP^{c} and VRQ14 Fab–ovPrP^{c} protein complexes (Fig. 3; for a sequence alignment of the variable regions of these Fab fragments, see Supplementary Fig. S2). Structural superpositions of the bound PrP^{c} in the different complexes indicate limited conformational variations among them (Table 2). The purportedly therapeutic antibody fragments ICSM18 Fab and POM1 Fab both recognize an epitope on or near to helix α1 of huPrP^{c}. The binding epitopes for these two antibodies are non-overlapping but lie in close proximity to one another. The Fab fragment of ICSM18 interacts with huPrP^{c} only through helix α1, and the residues of huPrP^{c} involved in this interaction are in the range 142–153 (Antonyuk *et al.*, 2009). Although both of the antibody Fab fragments, POM1 Fab and ICSM18 Fab, recognize adjacent huPrP^{c} epitopes, the modes of binding of the prion molecules to the respective cognate antibodies are completely different. The common huPrP^{c} epitope, helix α1, is bound to the Fab fragments of these antibodies in an opposite manner. Upon superimposing the Fab fragments of the POM1 and ICSM18 antibodies, the bound huPrP^{c} molecules in the respective CDRs are related to one another by an $\sim$180° rotation (Fig. 4).

The Fab fragment of VRQ14 binds to ovPrP^{c} in a completely different fashion and has a larger epitope that encompasses the N-terminal residues of helix α3 and the loop joining helix α2 and helix α3. This antibody recognizes a prion epitope that would be accessible in both PrP^{c} and PrP^{sc} (Eghiaian *et al.*, 2004). Previous structural studies on the VRQ14 Fab with ovPrP^{c} provides some crucial information on the secondary-structural rearrangement during the pathological conversion of PrP^{c} to PrP^{sc} (Eghiaian *et al.*, 2004). Compared with the interaction interface areas of the POM1 Fab–huPrP^{c} complex, larger buried surface areas are observed for the other two prion–antibody complexes: surface areas of 863 and 987 Å^{2}

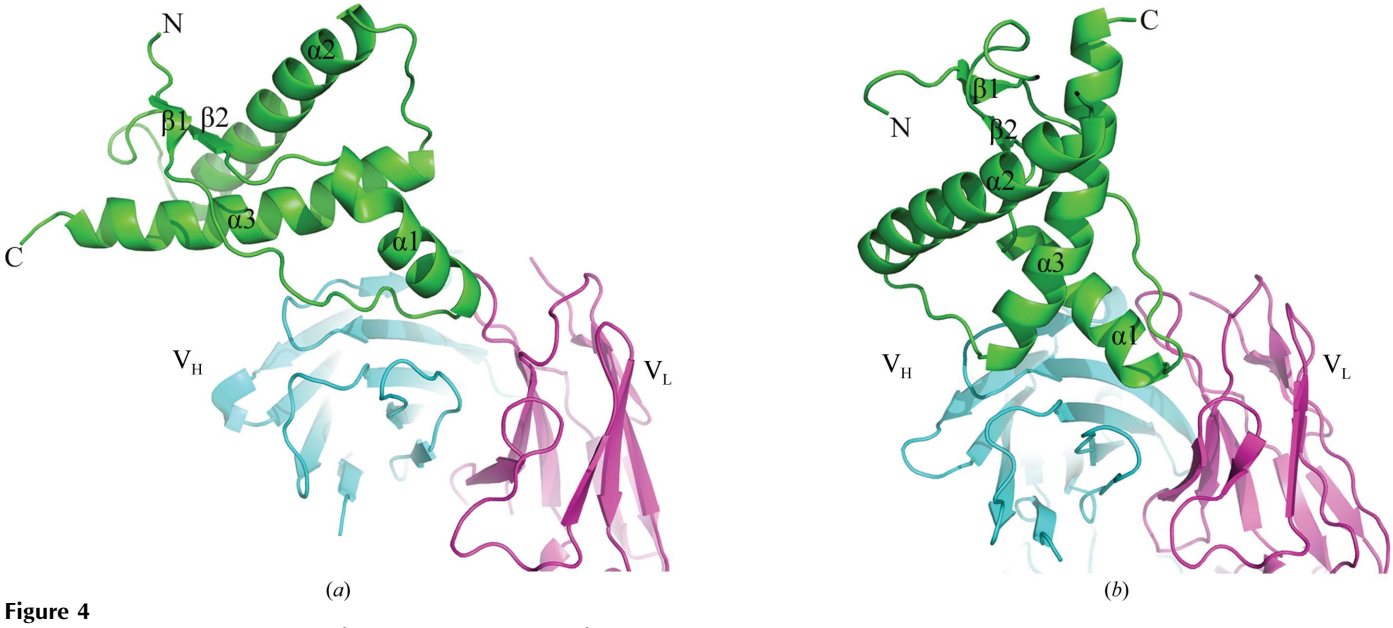

Figure 4
Structures of the POM1 Fab–huPrP^{c} and ICSM18 Fab–huPrP^{c} complexes are shown with identical orientations of the POM1 Fab and ICSM18 Fab antibody fragments. (*a*) Structure of POM1 Fab bound to huPrP^{c}. (*b*) Structure of ICSM18 Fab bound to huPrP^{c}. HuPrP^{c} is shown in green and the light chain and the heavy chain of the bound Fab fragments are represented in magenta and cyan, respectively. An $\sim$180° rotational shift of the bound huPrP^{c} is observed in the antibody–prion protein structures.

are buried in the ICSM18 Fab–huPrP^{c} and VRQ14 Fab–ovPrP^{c} complexes, respectively. Unlike the POM1 Fab–huPrP^{c} complex, in which the POM1 Fab heavy chain is the major interacting partner with huPrP^{c}, the interaction interface is evenly shared by the heavy chain and the light chain in the ICSM18 Fab–huPrP^{c} and VRQ14 Fab–ovPrP^{c} complexes. The nature of the interactions between the prion proteins and their cognate antibodies are quite variable among these prion–antibody complexes (Fig. 5). The molecular contacts between huPrP^{c} and ICSM18 are mostly electrostatic in nature. Three negatively charged patches are observed on the electrostatic surface map of ICSM18: one patch stabilizes the N-terminus of helix α3, the second patch stabilizes the N-terminus of helix α1 and the third patch is involved with Arg148 of helix α1. Three separately placed negatively charged residues on the ICSM18 Fab paratope form these charged centres: Asp31 and Asp35 from the ICSM18 Fab heavy chain and Asp49 from the ICSM18 Fab light chain contribute to the electrostatic stabilization of huPrP^{c}. The contact surface between huPrP^{c} and the POM1 Fab is partially electrostatic in nature; a broad negatively charged surface is present on the binding interface of the POM1 Fab and stabilizes the positive electrostatic potential mainly contributed by two residues, Arg208 and His140, of huPrP^{c}. A cluster of negatively charged residues on the POM1 Fab paratope, Asp52, Asp55, Asp73 and Glu74, contributes to this large patch of negatively charged surface. Unlike the polar interface area for ICSM18 and POM1, a broad hydrophobic interaction interface is observed for VRQ14. This paratope of the VRQ14 Fab forms a groove-like structure into which the ovPrP^{c} molecule fits owing to shape complementarity. Amongst the three prion–antibody complexes, the POM1 Fab–huPrP^{c} complex was found to be most stable based on the results of shape-complementary evaluation (Supplementary Table S2).

In the prion–antibody complexes, the flexibility of the bound PrP^{c} molecules is reduced significantly upon binding to their cognate antibody Fab fragments. Upon POM1 Fab binding, the regions of the huPrP^{c} protein that make contact with the POM1 Fab show reduced mobility compared with the rest of the structure; a reduction in temperature factor is

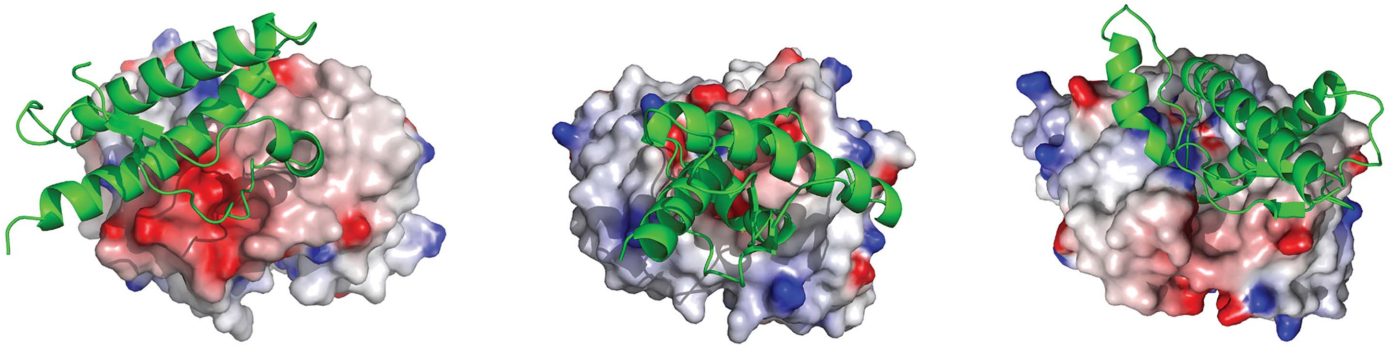

(*a*) (*b*) (*c*)

Figure 5
Surface representations of the Fab fragments based on the electrostatic potential of the residues constituting them. The electrostatic potential was calculated using the program *DelPhi* (Honig & Nicholls, 1995) with full charges assigned to Asp, Glu, Lys and Arg residues and partial charges assigned to the backbone atoms. The colour range extends from $-7kT$/e (red) to $+7kT$/e (blue). (*a*) Human prion protein bound to POM1 Fab. (*b*) Human prion protein bound to Fab ICSM18. (*c*) Sheep prion protein bound to VRQ14 Fab.

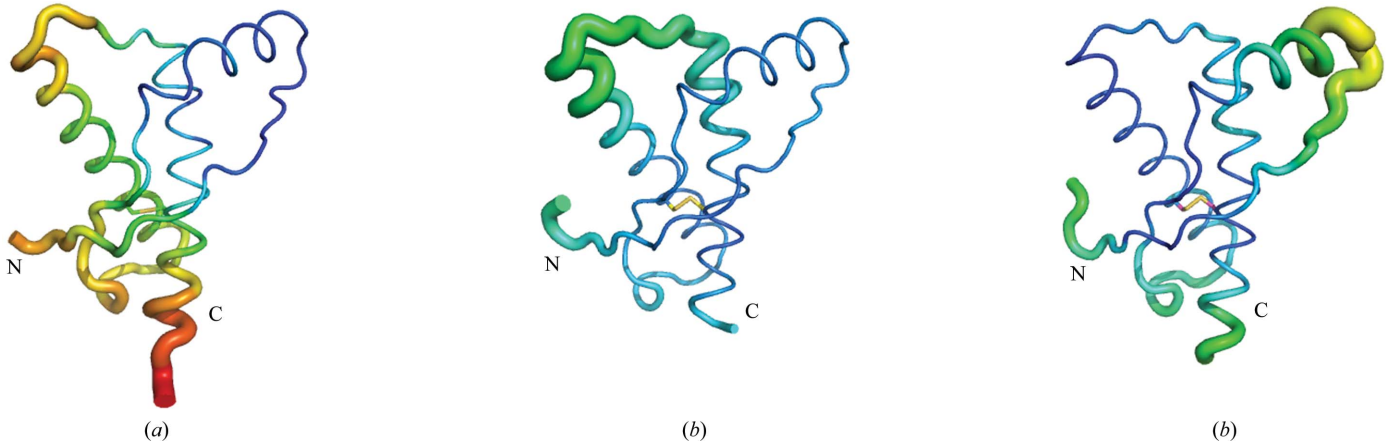

(*a*) (*b*) (*b*)

Figure 6
A representation of the thermal parameter distribution in prion proteins shown as *B*-factor 'putty' as implemented in *PyMOL* (http://www.pymol.org). The C$^{\alpha}$-atom *B* factors are depicted on the structure in dark blue (lowest *B* factor) through to red (highest *B* factor), with the radius of the ribbon increasing from low to high *B* factor. (*a*) Human prion protein from the POM1 Fab–huPrP^{c} complex. (*b*) Human prion protein from the ICSM18 Fab–huPrP^{c} complex. (*c*) Sheep prion protein from the VRQ14 Fab–ovPrP^{c} complex.

observed for these regions of huPrP^{c} (Fig. 6*a*). During the prion-misfolding process, helix α1 is considered to be the site that is primarily responsible for initiating the transformation of helical PrP^{c} into β-sheet-rich PrP^{sc}. This observation has been supported by several mutational analyses as well as by *in vitro* studies on helix α1 (Eghiaian *et al.*, 2004; Govaerts *et al.*, 2004). The binding of POM1 provides a stabilizing effect on helix α1 that should inhibit any structural changes in the prion protein. A lower temperature factor for this region of huPrP^{c} is observed because of POM1 Fab binding as well as ICSM18 Fab binding (Figs. 6*a* and 6*b*). The regions of huPrP^{c} protein that show a higher temperature factor in the ICSM18 Fab–huPrP^{c} complex are the C-terminal part of helix α2, the N-terminus of helix α3 and the loop joining helix α2 and helix α3. Unlike the N-terminus of helix α3 of the huPrP^{c} in the ICSM18 Fab–huPrP^{c} complex, this segment of huPrP^{c} makes contact with the POM1 Fab in the POM1 Fab–huPrP^{c} complex; therefore, a lower temperature factor is observed for this region. In the VRQ14 Fab–ovPrP^{c} complex a higher temperature factor is observed for helix α1 of ovPrP^{c}. This region of ovPrP^{c} remains on the opposite face to the part of ovPrP^{c} that makes contact with the VRQ14 Fab paratope in the VRQ14 Fab–ovPrP^{c} complex (Fig. 6*c*).

3.3. Binding studies of POM1 Fab with PrP^{c}

We have used isothermal titration calorimetry (ITC) to investigate the binding of the POM1 Fab antibody fragment to the C-terminal structured domain of huPrP^{c}. Titration of POM1 Fab into solution containing huPrP^{c} is shown in Fig. 7. The POM1 Fab binds to huPrP^{c} in a 1:1 ratio, with a dissociation constant of $4.5 \times 10^{-7}\,M$. The titration plot was derived from the integrated raw data and the solid line represents the best least-squares fit to these data. The variable parameters are best fitted using the following values: $n = 1.079 \pm 0.03$, $\Delta H = -12.0$ kJ mol^{-1} and $T\Delta S = -31.61$ kJ mol^{-1}. This binding event is an enthalpically driven process, as shown in Fig. 7. Although the antibody POM1 was specifically generated against recombinant moPrP^{c}, ELISA data indicate that the Fab fragment of this antibody recognizes PrP^{c}s from several different species, especially boPrP^{c} and ovPrP^{c}, which share a high sequence identity to moPrP^{c} as well as to huPrP^{c} (Supplementary Fig. S2 and Fig. S3). These data further suggest that the binding of the POM1 Fab to PrP^{c}s from other species are equally as strong as the binding of the POM1 Fab to huPrP^{c}.

4. Discussion

4.1. Structural analysis of the POM1 Fab–huPrP^{c} complex

The binding of the antiprion antibody POM1 relies on the tertiary structural fold of PrP^{c}, as previous ELISA studies on PrP^{c} peptide fragments spanning the binding epitope failed to show any binding (Polymenidou *et al.*, 2008). The POM1 Fab–huPrP^{c} structural data clearly demonstrate that a particular spatial arrangement of the discontinuous PrP^{c} epitope is essential in order to make contact with the POM1 paratope. The Fab fragment of the POM1 antibody can potentially recognize PrP^{c} from different species, especially those of boPrP^{c} and ovPrP^{c}, as observed from the ELISA data (Supplementary Fig. S4). The high sequence identity among the PrP^{c}s from several mammalian species, particularly in the POM1 epitope region, clearly explains the cross-species reactivity of this antibody. Interestingly, several antiprion monoclonal antibodies show varied affinity towards the pathogenic PrP^{sc} form along with their intrinsic binding properties towards the native PrP^{c} form. The VRQ14 antibody has previously been shown to recognize PrP^{sc} (Eghiaian *et al.*, 2004). Similarly, ICSM18 and POM1 can both recognize PrP^{sc} from scrapie-infected mouse brain homogenate, as demonstrated in previously reported immunoprecipitation experiments (Antonyuk *et al.*, 2009; Polymenidou *et al.*, 2008). This promiscuous nature of certain antibodies indicated either a certain degree of structural plasticity on the antigenic surfaces of PrP^{c} and PrP^{sc} or the structural conservation of the PrP^{c} molecules within the PrP^{sc} molecule, which is very unlikely.

Although the misfolding pathway that leads to PrP^{sc} formation is poorly understood, the existence of an aggregation-prone partially misfolded prion isoform, βPrP, and its

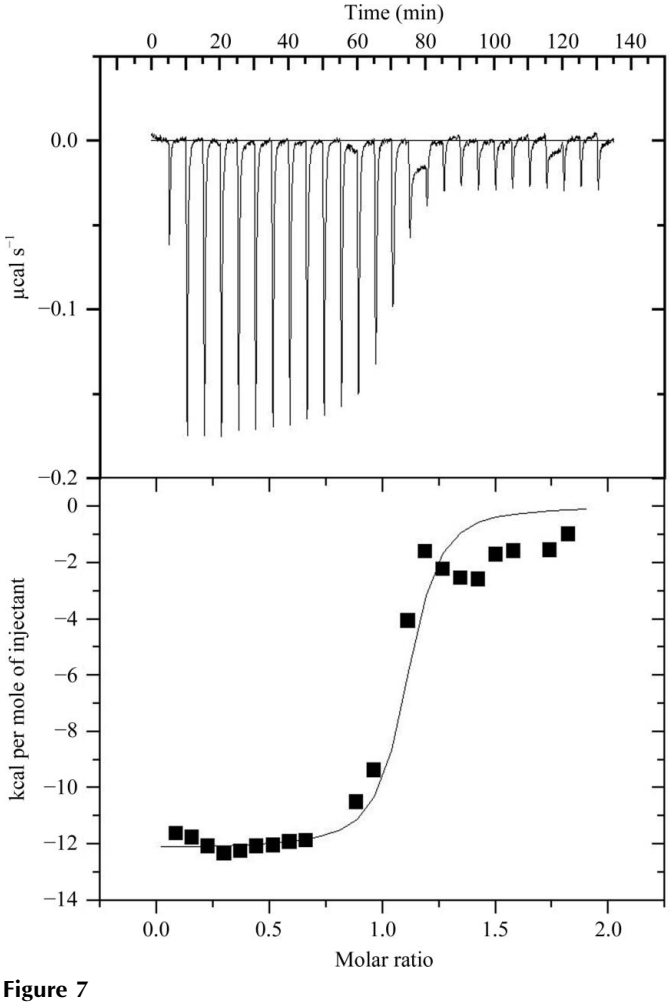

Figure 7
Isothermal titration calorimetry (ITC) measurements. Top, raw data from ITC experiments performed at 298 K. Bottom, integrated heat changes and the fitted curve based on a single-site model. 1 cal = 4.186 J.

involvement in PrP^{sc} seed generation has been the most widely accepted hypothesis to date (Govaerts *et al.*, 2004; Silveira *et al.*, 2005). In this context, it will be interesting to learn exactly what the initial oligomerization event of the βPrP molecules is that subsequently leads to PrP^{c} misfolding and aggregration. The intermolecular contacts that occur between neighbouring PrP^{c} molecules in a protein crystal through crystallographic symmetry-related arrangements could provide valuable information regarding this crucial oligomerization event. PrP^{c} molecules from several different species crystallized in a variety of different space groups and under different crystallization conditions have been observed to associate with each other through their antiparallel β-strands (Supplementary Fig. S5*a*). This four-stranded β-strand structure acquires elements of a steric zipper in which residues from two neighbouring β-strands are tightly interdigitated. This extended arrangement of β-strands functions as a nidus, or scaffold, for amyloid fibrils as well as for PrP^{sc} and this early phenomenon in scrapie generation has been extensively studied by Eisenberg and coworkers (Nelson *et al.*, 2005; Sawaya *et al.*, 2007). In the crystallographic symmetry-related arrangement of the ICSM18–$huPrP^{c}$ protein complex, the $huPrP^{c}$ molecules from neighbouring protein complexes are also arranged in a similar way (Antonyuk *et al.*, 2009). This structural result on the steric zipper association of $huPrP^{c}$ alone is not sufficient to explain the toxic aggregation process. This phenomenon has only been observed in short peptides; larger structural rearrangements are essential in the cases of larger proteins that unfold completely. However, this unique manner of PrP^{c} association may have some biological relevance. A different manner of oligomeric association has been observed for $huPrP^{c}$ in the crystallographic symmetry-related arrangement of the POM1 Fab–$huPrP^{c}$ complex (Supplementary Fig. S5*b*). The adjacent $huPrP^{c}$ molecules interact with one another through residues 136–138, which belong to the loop structure joining helix α1 and strand β1. This observation excludes the possibility of stacking around the β-strand region of $huPrP^{c}$ upon binding to POM1.

4.2. PrP^{c} binding and PrP^{sc} inhibition

Several small-molecule chemical compounds that bind tightly to the structured region of PrP^{c}, behave like chemical chaperones and inhibit PrP^{sc} formation have been described (Kuwata *et al.*, 2007; Hosokawa-Muto *et al.*, 2009). A recent investigation of a cationic tetrapyrrole [Fe(III)-TMPyP] compound that has been shown to reduce the levels of PrP^{sc} in scrapie-infected cells showed that it forms a 1:1 complex with the structured C-terminal part of $huPrP^{c}$; the dissociation constant measured for this interaction was 4.5 ± 2 μM (Nicoll *et al.*, 2010). Monoclonal antibodies have also been shown to have PrP^{sc}-reducing properties in the cellular model of prion propagation as well as in *in vivo* animal models (White *et al.*, 2003; Féraudet *et al.*, 2005). A correlation has been observed between the binding affinity of the antibody towards PrP^{c} and its potential for inhibiting PrP^{sc} propagation (Antonyuk *et al.*, 2009). In a comparative analysis of ICSM antibodies, their effectiveness towards PrP^{sc} reduction *versus* their binding potential towards PrP^{c} showed that the α-PrP-binding ICSM antibodies exhibited greater PrP^{sc} reduction compared with the β-PrP-binding ICSM antibodies because of their higher affinity for PrP^{c} (Antonyuk *et al.*, 2009). The K_{d} values for these ICSM series of monoclonal antibodies remained in the high-nanomolar to low-submicromolar range; these values were estimated by ELISA using recombinant PrP^{c}. The K_{d} value for POM1 Fab–$huPrP^{c}$ complex formation is 4.5×10^{-7} M and this medium-range binding affinity lies between the binding affinities estimated for the α-PrP-recognizing and the β-PrP-recognizing ICSM antibodies.

4.3. Structural implications of the antibody Fab–PrP^{c} complexes

In the three prion–antibody complexes analyzed in this study, the PrP^{c} epitopes recognized by these antibodies are quite distinct and non-overlapping. The paratopes for these different PrP^{c} epitopes are also comprised of unrelated structural features. Moreover, the molecular interactions observed for these prion–antibody associations are quite dissimilar in nature; electrostatic interactions predominate in the binding of ICSM18 and POM1 to their respective $huPrP^{c}$ molecules, while the interactions observed for VRQ14 with $ovPrP^{c}$ are primarily hydrophobic in nature, although several hydrogen bonds are present between the interacting partners. Despite these marked differences, formation of stable prion–antibody complexes is observed upon antibody binding. In addition to the tight binding properties, *in vivo* accessibility of the PrP^{c} motif to these antiprion antibodies is another important aspect that must be considered carefully in designing potential therapeutic products. The presence of two glycosylation sites, residues Asn181 and Asn197 of $huPrP^{c}$, as well as the C-terminal GPI anchor, might conceivably hinder the accessibility of an antiprion antibody to its PrP^{c} epitope in a natively folded conformation. The recombinant PrP^{c}s used in the structural studies of these three prion–antibody complexes are devoid of glycosylation. Although glycosylated native PrP^{c} and PrP^{c}s from recombinant sources both possess identical structural folds (Hornemann *et al.*, 2004), the spatial orientation of the glycan chain could limit the prion–antibody association *in vivo*. Hence, structural information regarding the two glycosylation sites of PrP^{c} in reference to the binding epitope of an antibody is extremely important in predicting the biological role of this antibody. Antibody ICSM18 recognizes the $huPrP^{c}$ epitope helix α1; however, one of the glycosylation sites on $huPrP^{c}$, Asn197, comes into close proximity of the paratope of this antibody (Fig. 3*b*). Although POM1 binds to the same helix α1 epitipe, its binding epitope is mainly the N-terminus of helix α1 and the loop preceding helix α1. Therefore, a different mode of binding of the POM1 Fab to $huPrP^{c}$ results in the globular domain of the $huPrP^{c}$ being rotated by $\sim 180^{\circ}$ relative to its orientation in the antigen-combining site of ICSM18 Fab (Fig. 4). This different orientation of $huPrP^{c}$ in the POM1 Fab results in both glycosylation sites of $huPrP^{c}$ facing away from the POM1 Fab and into the

surrounding solution (Figs. 3*a* and 3*b*). Thus, there is no steric interference from either of the covalently attached carbohydrate residues on huPrP^{c} with the POM1 Fab or the POM1 monoclonal antibody. Like ICSM18, the epitope recognized by VRQ14 is immediately adjacent to Asn200, which is one of the two sites of glycosylation on ovPrP^{c} (Fig. 3*c*).

These structural results for the protein complexes analyzed in this study have several important implications. Firstly, the bound conformation observed in the crystals of POM1 Fab–huPrP^{c} will be the same as those that would be adopted by the POM1 Fab or the POM1 IgG1 when bound *in vivo*. This observation is well supported by an *in vivo* experimental study on mouse brain slices, which indicated that POM1 IgG1 can readily recognize prion proteins in a physiologically relevant system (Polymenidou *et al.*, 2008). Secondly, the K_{d} that has been measured for the binding of POM1 Fab to huPrP^{c} should also be the same for the *in vivo* situation. On the other hand, the binding of ICSM18 Fab or its IgG and of VRQ14 Fab or its IgG will have at least two different conformations *in vivo* and will quite likely have two different corresponding K_{d} values. The conformation of ICSM18 Fab bound to huPrP^{c} will only be the same *in vivo* as that observed in the crystal structure for the unglycosylated form of huPrP^{c} and the monoglycosylated form (Asn181) of huPrP^{c}. The monoglycosylated huPrP^{c} (Asn197) and the diglycosylated huPrP^{c} will both present a strong steric clash with either the ICSM18 Fab or the ICSM18 IgG so that the binding mode is certain to be perturbed and different from that observed in the crystal structure. The loop structures on the ICSM18 Fab paratope could adopt conformations that would possibly relieve the steric clash that would result from the presence of carbohydrate residues on Asn197. This altered *in vivo* binding of ICSM18 Fab to huPrP^{c} would certainly be associated with an altered value of K_{d} and very likely a less avid interaction than that measured for the recombinant huPrP^{c}. Similarly, a less avid interaction resulting from a perturbed binding mode can be predicted for *in vivo* association of the VRQ14 Fab or its IgG with native ovPrP^{c}.

5. Conclusions

The crystal structure of the POM1 Fab–huPrP^{c} complex was determined at 2.4 Å resolution. It demonstrates that the POM1 Fab binds to the structured domain of huPrP^{c} through a discontinuous epitope comprised of a loop between strand $\beta1$ and helix $\alpha1$, the N-terminus of helix $\alpha1$ and three residues from helix $\alpha3$. This POM1 epitope is also in close vicinity to the epitope recognized by the purportedly therapeutic antibody ICSM18. The measured K_{d} value for the association of POM1 Fab and huPrP^{c} remains midway between the K_{d} values observed for the ICSM series of therapeutic antibodies. Therefore, a similar functional role can be predicted for POM1. Structural analysis of the three prion–antibody complexes presented here is a step forward towards understanding the interplay of hydrogen bonding and other molecular interactions between prion proteins and their cognate monoclonal antibodies. There is a diverse nature of molecular interactions that are responsible for association between the paratopes and the epitopes. This knowledge will further facilitate the design of better prion-protein binders through an antibody-engineering approach. Although the structural data presented here are based on prion proteins from recombinant sources, many meaningful conclusions can be derived on the *in vivo* associations of glycosylated prion proteins and these antibodies. However, detailed structural studies are needed on the glycosylated native forms of the prion proteins along with their cognate antiprion antibodies in order to better illustrate the proposed mechanism of *in vivo* accessibility and binding.

This work has been funded by PrioNet Canada and AHFMR in grants to MNGJ. The data collection described in this paper was performed at the Canadian Light Source, which is supported by the Natural Sciences and Engineering Research Council of Canada, the National Research Council Canada, the Canadian Institutes of Health Research, the Province of Saskatchewan, Western Economic Diversification Canada and the University of Saskatchewan. The prion clones were generously provided by the PrioNet Prion Protein and Plasmid Production Facility, University of Alberta.

References

Afonine, P. V., Grosse-Kunstleve, R. W., Echols, N., Headd, J. J., Moriarty, N. W., Mustyakimov, M., Terwilliger, T. C., Urzhumtsev, A., Zwart, P. H. & Adams, P. D. (2012). *Acta Cryst.* D**68**, 352–367.
Aguzzi, A. & Polymenidou, M. (2004). *Cell*, **116**, 313–327.
Antonyuk, S. V., Trevitt, C. R., Strange, R. W., Jackson, G. S., Sangar, D., Batchelor, M., Cooper, S., Fraser, C., Jones, S., Georgiou, T., Khalili-Shirazi, A., Clarke, A. R., Hasnain, S. S. & Collinge, J. (2009). *Proc. Natl Acad. Sci. USA*, **106**, 2554–2558.
Baral, P. K., Wieland, B., Swayampakula, M., Polymenidou, M., Aguzzi, A., Kav, N. N. V. & James, M. N. G. (2011). *Acta Cryst.* F**67**, 1211–1213.
Bradford, M. M. (1976). *Anal. Biochem.* **72**, 248–254.
Calella, A. M., Farinelli, M., Nuvolone, M., Mirante, O., Moos, R., Falsig, J., Mansuy, I. M. & Aguzzi, A. (2010). *EMBO Mol. Med.* **2**, 306–314.
Castilla, J., Saá, P., Hetz, C. & Soto, C. (2005). *Cell*, **121**, 195–206.
Collinge, J. (2001). *Annu. Rev. Neurosci.* **24**, 519–550.
Crowley, P. B. & Golovin, A. (2005). *Proteins*, **59**, 231–239.
Eghiaian, F., Grosclaude, J., Lesceu, S., Debey, P., Doublet, B., Tréguer, E., Rezaei, H. & Knossow, M. (2004). *Proc. Natl Acad. Sci. USA*, **101**, 10254–10259.
Emsley, P. & Cowtan, K. (2004). *Acta Cryst.* D**60**, 2126–2132.
Féraudet, C., Morel, N., Simon, S., Volland, H., Frobert, Y., Créminon, C., Vilette, D., Lehmann, S. & Grassi, J. (2005). *J. Biol. Chem.* **280**, 11247–11258.
Freir, D. B., Nicoll, A. J., Klyubin, I., Panico, S., Mc Donald, J. M., Risse, E., Asante, E. A., Farrow, M. A., Sessions, R. B., Saibil, H. R., Clarke, A. R., Rowan, M. J., Walsh, D. M. & Collinge, J. (2011). *Nature Commun.* **2**, 336.
Govaerts, C., Wille, H., Prusiner, S. B. & Cohen, F. E. (2004). *Proc. Natl Acad. Sci. USA*, **101**, 8342–8347.
Honig, B. & Nicholls, A. (1995). *Science*, **268**, 1144–1149.
Hornemann, S., Schorn, C. & Wüthrich, K. (2004). *EMBO Rep.* **5**, 1159–1164.
Hosokawa-Muto, J., Kamatari, Y. O., Nakamura, H. K. & Kuwata, K. (2009). *Antimicrob. Agents Chemother.* **53**, 765–771.
Hosszu, L. L., Trevitt, C. R., Jones, S., Batchelor, M., Scott, D. J., Jackson, G. S., Collinge, J., Waltho, J. P. & Clarke, A. R. (2009). *J. Biol. Chem.* **284**, 21981–21990.

Kessels, H. W., Nguyen, L. N., Nabavi, S. & Malinow, R. (2010). *Nature (London)*, **466**, E3–E5.
Klöhn, P. C., Farmer, M., Linehan, J. M., O'Malley, C., Fernandez de Marco, M., Taylor, W., Farrow, M., Khalili-Shirazi, A., Brandner, S. & Collinge, J. (2012). *Science*, **335**, 52.
Knaus, K. J., Morillas, M., Swietnicki, W., Malone, M., Surewicz, W. K. & Yee, V. C. (2001). *Nature Struct. Biol.* **8**, 770–774.
Kuwata, K., Nishida, N., Matsumoto, T., Kamatari, Y. O., Hosokawa-Muto, J., Kodama, K., Nakamura, H. K., Kimura, K., Kawasaki, M., Takakura, Y., Shirabe, S., Takata, J., Kataoka, Y. & Katamine, S. (2007). *Proc. Natl Acad. Sci. USA*, **104**, 11921–11926.
Lee, S., Antony, L., Hartmann, R., Knaus, K. J., Surewicz, K., Surewicz, W. K. & Yee, V. C. (2010). *EMBO J.* **29**, 251–262.
Leslie, A. G. W. (2006). *Acta Cryst.* D**62**, 48–57.
Nelson, R., Sawaya, M. R., Balbirnie, M., Madsen, A. Ø., Riekel, C., Grothe, R. & Eisenberg, D. (2005). *Nature (London)*, **435**, 773–778.
Nicoll, A. J., Trevitt, C. R., Tattum, M. H., Risse, E., Quarterman, E., Ibarra, A. A., Wright, C., Jackson, G. S., Sessions, R. B., Farrow, M., Waltho, J. P., Clarke, A. R. & Collinge, J. (2010). *Proc. Natl Acad. Sci. USA*, **107**, 17610–17615.
Polymenidou, M. *et al.* (2008). *PLoS One*, **3**, e3872.
Ramaraj, T., Angel, T., Dratz, E. A., Jesaitis, A. J. & Mumey, B. (2012). *Biochim. Biophys. Acta*, **1824**, 520–532.
Sawaya, M. R., Sambashivan, S., Nelson, R., Ivanova, M. I., Sievers, S. A., Apostol, M. I., Thompson, M. J., Balbirnie, M., Wiltzius, J. J., McFarlane, H. T., Madsen, A. Ø., Riekel, C. & Eisenberg, D. (2007). *Nature (London)*, **447**, 453–457.
Sigurdson, C. J., Nilsson, K. P., Hornemann, S., Heikenwalder, M., Manco, G., Schwarz, P., Ott, D., Rülicke, T., Liberski, P. P., Julius, C., Falsig, J., Stitz, L., Wüthrich, K. & Aguzzi, A. (2009). *Proc. Natl Acad. Sci. USA*, **106**, 304–309.
Silveira, J. R., Raymond, G. J., Hughson, A. G., Race, R. E., Sim, V. L., Hayes, S. F. & Caughey, B. (2005). *Nature (London)*, **437**, 257–261.
Sinha, N. & Smith-Gill, S. J. (2002). *Curr. Protein Pept. Sci.* **3**, 601–614.
Smirnovas, V., Baron, G. S., Offerdahl, D. K., Raymond, G. J., Caughey, B. & Surewicz, W. K. (2011). *Nature Struct. Mol. Biol.* **18**, 504–506.
Solforosi, L., Criado, J. R., McGavern, D. B., Wirz, S., Sánchez-Alavez, M., Sugama, S., DeGiorgio, L. A., Volpe, B. T., Wiseman, E., Abalos, G., Masliah, E., Gilden, D., Oldstone, M. B., Conti, B. & Williamson, R. A. (2004). *Science*, **303**, 1514–1516.
Vagin, A. & Teplyakov, A. (2010). *Acta Cryst.* D**66**, 22–25.
White, A. R., Enever, P., Tayebi, M., Mushens, R., Linehan, J., Brandner, S., Anstee, D., Collinge, J. & Hawke, S. (2003). *Nature (London)*, **422**, 80–83.
Will, R. G. (1999). *J. R. Coll. Physicians Lond.* **33**, 311–315.
Winn, M. D. *et al.* (2011). *Acta Cryst.* D**67**, 235–242.
Yin, S.-M., Zheng, Y. & Tien, P. (2003). *Protein Expr. Purif.* **32**, 104–109.
Zahn, R., Liu, A., Lührs, T., Riek, R., von Schroetter, C., López García, F., Billeter, M., Calzolai, L., Wider, G. & Wüthrich, K. (2000). *Proc. Natl Acad. Sci. USA*, **97**, 145–150.